Polym. Bull. (2012) 68:1707–1720
DOI 10.1007/s00289-011-0674-x

ORIGINAL PAPER

Preparation, characterization, and in vitro release of folic acid-conjugated chitosan nanoparticles loaded with methotrexate for targeted delivery

Jingou Ji · Danjun Wu · Li Liu · Jida Chen · Yi Xu

Received: 15 June 2011 / Revised: 22 October 2011 / Accepted: 27 November 2011 /
Published online: 3 December 2011

Abstract To reduce the toxicity of methotrexate (MTX) and increase the targeting of nanoparticles, the MTX-loaded chitosan (CS) covalently bonded with folic acid (FA) nanoparticles were prepared, and sodium tripolyphosphate was used as the cross-linking agent. FA was successfully conjugated to CS confirmed by ^{1}H-NMR and Fourier transform infrared spectrometer (FT-IR). The prepared FA–CS nanoparticles were characterized by FT-IR spectroscopy to confirm the cross-linking reaction between FA–CS and cross-linking agent. X-ray diffraction was performed to reveal the crystalline nature of the drug after encapsulation. The average diameters of the nanoparticles ranged from 293.9 ± 24.2 to 401.5 ± 20.4 nm with a narrow particle size distribution. In vitro release pattern in phosphate buffer saline (pH 6.8) indicated that the characteristics of the MTX-loaded nanoparticles appeared to have an initial burst effect and followed by a slow, sustained drug release. FA or low molecular weight FA conjugate fragments were also released from the nanoparticles, which might have potential to reduce toxic effects of MTX within the body.

Keywords Chitosan · Folic acid · Methotrexate · Nanoparticles · Targeted delivery

Introduction

Methotrexate (MTX), a dihydrofolate reductase inhibitor, is one of the most widely used drugs for the treatment of various neoplastic diseases including leukemia, osteosarcoma, lymphoma, breast cancer, and so on [1]. However, undesirable side effects of MTX have been reported such as neurotoxicity and other related toxicity to normal cells [2].

J. Ji (✉) · D. Wu · L. Liu · J. Chen · Y. Xu
Chongqing, China
e-mail: jingou_ji@yahoo.com.cn

Polymeric nanoparticles have been widely used as the drug carriers for the controlled release of the drugs [3–5], which greatly reduced unwanted side effects and improve the treatment efficacy [6, 7]. Polymeric materials, such as chitosan (CS), poly (L-lactic acid) (PLLA), and poly-D,L-lactide-*co*-glycolide (PLGA) are used for the synthesis of nanoparticles. Among them, CS has been shown to be a useful natural biopolymer for nanoparticles because of its unique properties, such as mucoadhesivity, biocompatibility, nontoxicity, biodegradability, and ability to enhance the paracellular transport of drugs [8–11]. However, CS nanoparticles are restricted due to the low efficiency of specific targeting. An effective approach to improve the targeting capability is to conjugate nanoparticles with chemical or biological reagents including antibodies or low molecular weight targeting agents, such as folic acid (FA) [12]. FA is generally recognized as an effective tumor targeting agent to conjugate with nanoparticles because of its specific binding with the folate receptors (FRs) [13]. FA conjugates, which are covalently derivatized via its γ-carboxyl moiety, can retain the high affinity ligand binding property of FA ($K_d \sim 10^{-9}$ M), and the kinetics of cellular uptake of conjugated FA compounds by FRs is similar to that of free FA [14]. In addition, published data supported the contention that neurotoxicity can be prevented by adequate FA or folinic acid rescue even after very high doses of MTX [15–17].

In this study, MTX-incorporated FA–CS nanoparticles were prepared. The physicochemical properties of the nanoparticles were investigated and the in vitro release behaviors of drug-loaded FA–CS nanoparticles and blank FA–CS nanoparticles without loading drug were described.

Experimental

Materials

Chitosan (CS, Deacetylation degree of 95% and molecular weight of 80 kDa) was purchased from Golden-shell Biochemical Co. Ltd. (Zhejiang, China). Sodium tripolyphosphate (TPP) was purchased from Wenzhou Dongsheng Chemical reagent Co. Ltd. (Zhejiang, China). MTX was supplied from Shaanxi Top Pharm Chemical Co. Ltd. (Shaanxi, China). FA, *N*,*N*'-dicyclohexylcarbodiimide (DCC), *N*-hydroxysuccinimide (NHS) were purchased from Sinopharm Chemical Reagent Co. Ltd. (shanghai, China). All other materials and reagents used in the study were of analytical grades.

Synthesis of NHS-ester of FA

NHS-ester of FA was synthesized according to the method previously reported [18] with slight changes. The synthesis process of NHS-ester of FA is presented in Fig. 1a. In brief, 1.0 g of FA was dissolved in 20 mL dimethylsulfoxide (DMSO). 1.1 Molar excess of NHS and DCC and 1.5 mL triethylamine were then added. The reaction was allowed to proceed for 12 h under stirring in the dark. The by-product dicyclohexylurea was removed by filtration. Then, yellow NHS-ester of FA was

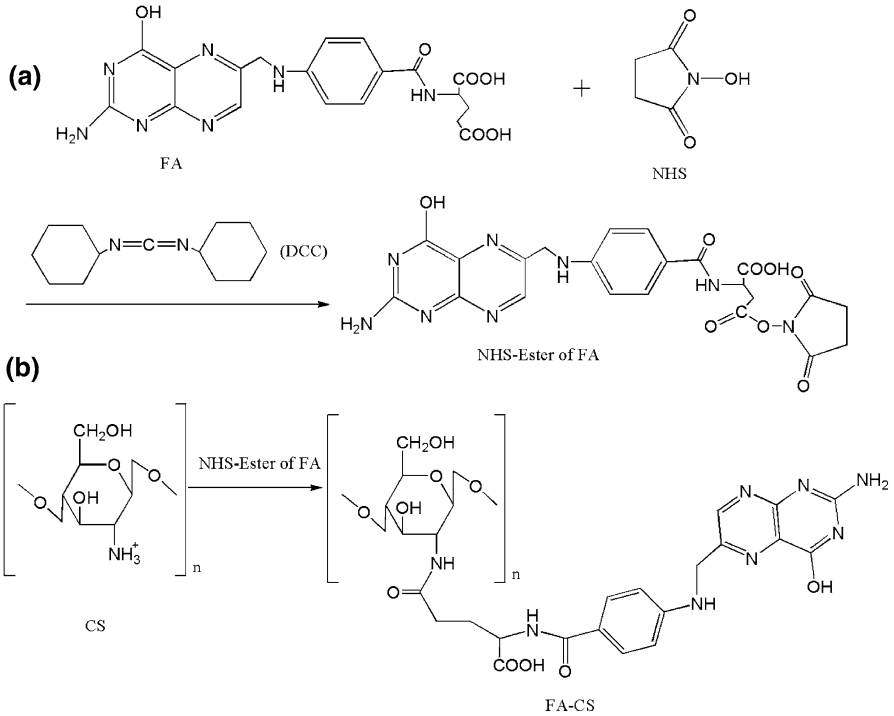

Fig. 1 The procedure for the synthesis of FA–CS: synthesis process of NHS-ester of FA (*a*); synthesis process of FA–CS (*b*)

precipitated and washed repeatedly in cold anhydrous ether contained 30% acetone. The product was dried under vacuum at room temperature.

Synthesis of FA–CS conjugate

The reaction course of FA–CS conjugate was as follows: 40 mg of CS was dissolved in 10 mL of acetate buffer (pH 4.7), and an equivalent amount of NHS-ester of FA in anhydrous DMSO was then dropwise added to the above CS solution. The resulting mixture was stirred at 30 °C in the dark for 16 h. The solution was brought to pH 9.0 by dripping with NaOH aqueous solution (1.0 M). To eliminate unbound FA and isolate the conjugated polymers, the reaction mixtures were dialyzed (molecular weight cut-off = 8–14 kDa) against phosphate buffer pH 7.4 for 3 days and then against water for 3 days [19, 22]. The polymer was isolated by lyophilization.

Characterization of FA–CS conjugate

The ^{1}H-NMR spectra of CS and FA–CS conjugate were recorded on a 500 MHz NMR spectrometer (AVANCE 500, Bruker, Rheinstetten, Germany) using CF_3COOD/D_2O mixture (0.1 mL CF_3COOD in 0.5 mL D_2O) as a solvent. The

degree of substitution (DS) of FA to monosaccharide residue of CS was calculated based on ^{1}H-NMR spectrum of FA–CS conjugate.

Preparation of polymer FA–CS nanoparticles

Polymer FA–CS nanoparticles were prepared by ionic cross-linking with TPP. FA–CS solution (0.2%, w/v) was dissolved in dilute acetic acid (2%, v/v) at room temperature and adjusted to pH 5.0 by dropwise addition of dilute NaOH. TPP solution (0.4%, w/v) added slowly to FA–CS solution under mild magnetic stirring till stable nanoparticles suspensions were obtained. MTX-encapsulated nanoparticles were prepared in the similar way. The FA–CS solution(0.2%, w/v) was adjusted to different pH (4.0, 4.5, 5.0, and 5.5) and different amount of MTX solution dissolving in DMSO (mass ratios of MTX to polymer were 1:20, 2:20, 3:20, and 4:20) was added slowly to previous FA–CS solution with sonication. The nanoparticles were spontaneously formed upon addition of the TPP solution. The different mass ratios of TPP to FA–CS ranging from 1:7 to 1:4 were investigated. The nanoparticles suspensions were continuously stirred for half an hour and centrifuged at 16,000 rpm for 30 min. The resulting nanoparticles were lyophilized and stored.

Characterization of the MTX/FA–CS nanoparticles

The surface morphology of the MTX encapsulated FA–CS nanoparticles was characterized using scanning electron microscope (SEM) (Philips, FEINova 400 Nano SEM, Dutch). The nanoparticles suspensions were spread on a glass plate and dried at room temperature. The dried nanoparticles were then coated with gold metal under vacuum and then examined.

The mean particle size, zeta potential, and polydispersity index (PDI) of the prepared FA–CS nanoparticles were measured by photon correlation spectroscopy using nano ZS90 Zetasizer (Malvern Instruments, UK).

The chemical structure and complexes formation of CS, FA–CS, and drug-loaded FA–CS nanoparticles were analyzed by Fourier transform infrared spectrometer (FT-IR, Nicolet, 5DX/550II, USA). The samples used for the FT-IR spectroscopic characteristics were prepared by grinding the dry specimens with KBr and pressing the mixed powder to form disks.

X-ray diffraction (XRD) was recorded by a Shimadzu Lab-XRD-6000 diffractometer and used a Cu-K_{α} as target at 40 kV and 30 mA.

Evaluation of drug-loading capacity (LC) and yield of the nanoparticles

In the determination of the LC, the MTX-loaded FA–CS nanoparticles were separated from the aqueous suspension medium by centrifugation at 16,000 rpm for 30 min. The content of free MTX in the supernatants was determined by UV spectrophotometer at 303 nm using supernatant of their corresponding blank nanoparticles without loaded drugs as basic correction. Each batch samples were measured in triplicate. The pellets after centrifugation were lyophilized and weighed

to calculate the LC and the yield. The LC and yield were calculated by following Eqs. 1 and 2, respectively:

$$\text{LC} = \frac{\text{Total amount of MTX} - \text{free amount of MTX}}{\text{Weight of nanoparticles}} \times 100\%, \quad (1)$$

$$\text{Yield} = \frac{\text{Weight of nanoparticles}}{\text{Weight of total components}} \times 100\%. \quad (2)$$

Measurement of the storage stability of nanoparticles

The stability of the FA–CS nanoparticles was tested as a function of pH 5, 6, 6.8, and 7.4. Fresh FA–CS nanodispersion samples were separately added to 50 mL different pH buffer solutions (5, 6, 6.8, and 7.4). The samples were stored at room temperature. The light transmittance was measured at 500 nm by UV/Vis spectrophotometer at scheduled time intervals [20].

In vitro release study of the nanoparticles

In vitro release study of the drug-loaded nanoparticles and blank nanoparticles were studied in vitro by dialysis method in phosphate buffered saline (PBS, pH 6.8). In brief, the lyophilized drug-loaded nanoparticles (50 mg) were dispersed in 5 mL of PBS (pH 6.8) and the dispersed FA–CS nanoparticles were placed into dialysis tube (molecular weight cut-off 8–14 kDa; Spectrum®) that immersed into 50 mL PBS solution. The system was shaken at 100 rpm at 37 °C. At pre-defined time intervals, the release media were collected and replaced with equivalent fresh release media. Triplicate samples were analyzed at each time point.

The release of FA from the blank nanoparticles was treated similarly to the drug-loaded nanoparticles. The concentration of the released MTX and FA into PBS were determined by UV spectrophotometer at 303 and 358 nm, respectively.

Results and discussion

Synthesis and characterization of FA–CS conjugate

FA was conjugated to CS following the usual NHS/DCC reaction to get FA–CS conjugate. Though FA has two –COOH groups at the end positions and it has already been established that γ-COOH of FA is more prone to this reaction due to its higher reactivity [21]. Final product FA–CS was synthesized by the reaction between the activated FA ester and the primary amine groups of CS through the formation of amide bond under homogeneous conditions (Fig. 1). The structure of grafting FA was confirmed by ^{1}H-NMR spectroscopy as shown in Fig. 2. The peaks at 2.07 ppm attributed to the acetamino group CH_3 and CH peak appeared at 3.50–3.95 ppm, corresponding to carbons 3, 4, 5, and 6 of glucosamine ring of CS (Fig 2b). Coupling of FA to CS residue was confirmed by the appearance of the peculiar signals at 7.60 and 6.40 ppm, which attributed to the aromatic protons of

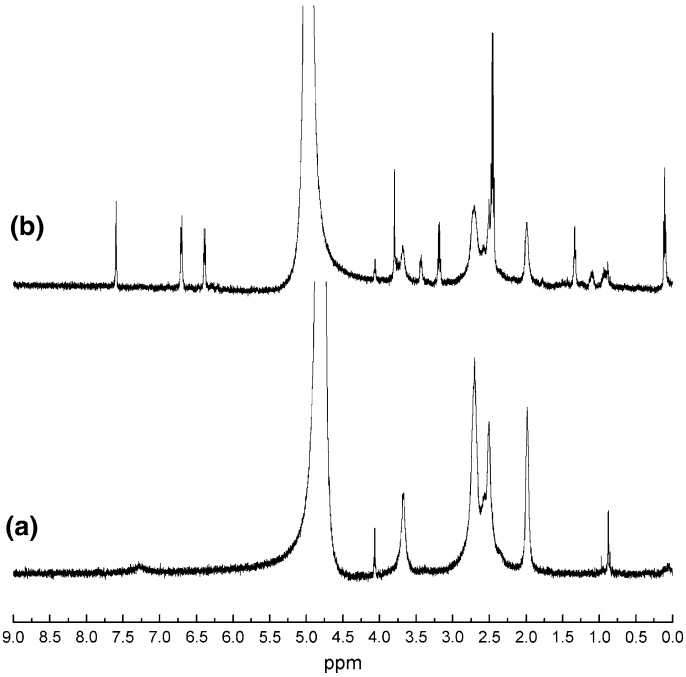

Fig. 2 ^{1}H-NMR spectra of CS (*a*) and FA–CS conjugate (*b*)

FA, and characteristic peaks at 6.72 and 2.45 ppm corresponded to the FA proton from the H10 and H22, respectively [22, 23]. DS value of FA was determined from the relative ratio of the peak area of carbon 12/16 of FA at 6.40 ppm and the peak area of carbon 5 of FA–CS at 3.60 ppm. After calculation, the DS of FA to monosaccharide residue of CS was 11.2%.

Preparation of MTX-loaded FA–CS nanoparticles

The cross-linking reaction of FA–CS nanoparticles occurs due to the ionic interaction between free protonated amino group ($-NH_3^+$) of the FA–CS and anions of TPP.

Preparation of the drug-loaded FA–CS nanoparticles with different mass ratios of TPP to FA–CS from 1:7 to 1:4 was investigated. As the pH value of FA–CS solution (0.2%, w/v) was selected as 5.0 and mass ratio of MTX to FA–CS was fixed to 3:20, the effects of the TPP/FA–CS mass ratio on the physicochemical properties of prepared nanoparticles are shown in Table 1. It was found that the LC and yield of the nanoparticles increased with an increase of TPP to FA–CS mass ratio. This trend could be explained by the fact that larger amount of TPP could enhance the cross-linking degree between the amino group of FA–CS and TPP anions, and this leads to more capacity to encapsulate drugs. The particle size distribution and zeta potential of the nanoparticles were also investigated in this study. A gradual increase in the particle size from 293.9 ± 24.2 to 375.3 ± 21.6 nm and gradual decrease in zeta

Table 1 Effects of different TPP to FA–CS mass ratios on the physicochemical properties of the FA–CS nanoparticles (mean ± SD, $n = 3$)

TPP/FA–CS mass ratio	LC (%)	Yield (%)	Particle size (nm)	PDI	Zeta potential (mV)
1:7	7.33 ± 0.09	27.36 ± 2.91	293.9 ± 24.2	0.180 ± 0.008	37.46 ± 2.95
1:6	9.87 ± 0.25	31.58 ± 2.51	309.7 ± 20.9	0.239 ± 0.052	31.58 ± 1.72
1:5	10.46 ± 0.14	38.89 ± 2.53	358.2 ± 15.6	0.224 ± 0.040	23.81 ± 1.85
1:4	11.02 ± 0.33	57.14 ± 3.38	375.3 ± 21.6	0.219 ± 0.036	22.84 ± 2.07

potential from 37.46 ± 2.95 to 22.84 ± 2.07 mV with the increase of TPP/FA–CS mass ratio were noted.

The FA–CS nanoparticles with different drug-to-polymer ratios (from 1:20 to 4:20) were also prepared. Table 2 demonstrates that LC of nanoparticles increased from 3.85 ± 0.05 to 11.54 ± 0.31% with the increase of drug-to-polymer ratio, which indicated that higher drug concentration in the polymer matrix is prone to increase the LC of nanoparticles. However, the polymer itself may have a limited capacity to encapsulate a specific drug. Beyond its maximum capacity, more drugs might be wasted during the fabrication process [24]. The particle size gradually increased and a slight decrease in the zeta potential was observed with the increase of the drug-to-polymer ratio. No significant change was observed in the nanoparticle yield.

The effects of different pH values of FA–CS solution (from 4.0 to 5.5) on the characteristics of nanoparticles are shown in Table 3. It demonstrates that the zeta potential of the nanoparticles decreased from 31.48 ± 2.32 to 22.84 ± 1.79 mV

Table 2 Effects of drug MTX to FA–CS mass ratios on the physicochemical properties of the FA–CS nanoparticles (mean ± SD, $n = 3$)

MTX/FA–CS mass ratio	LC (%)	Yield (%)	Particle size (nm)	PDI	Zeta potential (mV)
1:20	3.85 ± 0.05	34.80 ± 2.21	325.4 ± 18.0	0.211 ± 0.046	24.67 ± 1.83
2:20	6.83 ± 0.13	38.08 ± 3.12	340.5 ± 22.5	0.220 ± 0.032	24.29 ± 1.62
3:20	10.46 ± 0.14	38.89 ± 2.53	358.2 ± 15.6	0.224 ± 0.040	23.81 ± 1.85
4:20	11.54 ± 0.31	38.21 ± 2.44	401.5 ± 20.4	0.181 ± 0.039	23.57 ± 1.68

Table 3 Effects of pH value of FA–CS solution on the physicochemical properties of the FA–CS nanoparticles (mean ± SD, $n = 3$)

pH value	LC (%)	Yield (%)	Particle size (nm)	PDI	Zeta potential (mV)
4.0	3.28 ± 0.10	34.07 ± 4.16	316.9 ± 16.9	0.229 ± 0.034	31.48 ± 2.32
4.5	6.97 ± 0.07	37.04 ± 3.37	329.2 ± 13.3	0.295 ± 0.049	29.04 ± 2.29
5.0	10.46 ± 0.14	38.89 ± 2.53	358.2 ± 15.6	0.224 ± 0.040	23.81 ± 1.85
5.5	7.79 ± 0.11	57.78 ± 4.36	394.1 ± 23.0	0.256 ± 0.032	22.84 ± 1.79

with the increase of solution pH, which may be related to the decrease of the positive charges of FA–CS. When the pH of FA–CS was up to 5.5, the ionization degree of amine groups was decreased greatly. A higher LC of MTX was obtained at pH 5.0, which may be related to the sufficient anions of TPP and the positive charges of FA–CS, and hence enhanced the degree of cross-link reaction. The average particle size of the nanoparticles increased from 316.9 ± 16.9 to 394.1 ± 23.0 nm with the increase of solution pH, which probably attributed to the nanoparticles aggregation. The values of PDI were all smaller than 0.300, which indicated that the nanoparticles had a narrow particle size distribution [25].

Characterization of FA–CS nanoparticles

The morphological characteristics of the MTX-loaded FA–CS nanoparticles were examined by SEM shown in Fig. 3. The results suggest that the nanoparticles were homogeneously dispersed with an average size of about 300 nm.

Figure 4 depicts the FT-IR spectra of CS, FA–CS, and FA–CS nanoparticles. The CS spectrum (Fig. 4a) presents characteristic peaks at 3,426 cm^{-1} assigned to stretching vibration of $–NH_2$ and –OH groups, at 1,601 cm^{-1} ascribed to the N–H bending mode in the primary amine, at 1,078 cm^{-1} related to the C–O stretching vibration, and at 601 cm^{-1}, reflecting the pyranoside ring stretching vibration, in agreement with the literature [26]. Comparing with CS, the FA–CS spectrum (Fig. 4b) exhibits the appearance of –CONH amide band at 1,650 cm^{-1} and the N–H bending in the second amine at 1,575 cm^{-1}. The results indicate that –COOH of FA is conjugated to the amino of CS. In addition, the peak of 3,420 cm^{-1} of FA–CS becomes wider, indicating that hydrogen bonding has been enhanced between the FA and CS. For FA–CS nanoparticles (Fig. 4c), 1,601 cm^{-1} peak of $–NH_2$ bending vibration shifts to 1,552 cm^{-1} and a new sharp peak 1,630 cm^{-1} appears, which indicates the linkage between TPP and ammonium ion of the FA–CS. Moreover, the peak of 3,420 cm^{-1} becomes wider, which demonstrates that the inter- and intra-molecular action are enhanced in FA–CS nanoparticles because of the tripolyphosphoric groups of TPP linked with ammonium group of FA–CS [27].

Powder XRD patterns of CS, FA–CS, MTX, and the MTX-loaded FA–CS nanoparticles are illustrated in Fig. 5. There are two strong peaks in the diffractogram of CS at 2θ values of 11° and 20° (Fig. 5a) and several strong peaks in the diffractogram of MTX (Fig. 5d), indicating the high degree of crystallinity of CS and MTX. It is noted that the peaks at $2\theta = 11°$ and 20° decrease greatly in the newly prepared polymer FA–CS (Fig. 5b) as the crystallinity decreases than that of CS itself due to the deformation of the strong hydrogen bonds between CS and FA. Nearly, no peak is found in the diffractogram of the drug-loaded FA–CS nanoparticles. XRD of the FA–CS nanoparticles (Fig. 5c) is characteristic of an amorphous polymer. The nanoparticles are composed of a dense network structure of interpenetrating polymer chains crosslinked to one another by TPP counterions. XRD implicates greater disarray in the chain alignment in the nanoparticles after the crosslinks [28]. In addition, the characteristic peaks of MTX disappear in those corresponding to drug-loaded

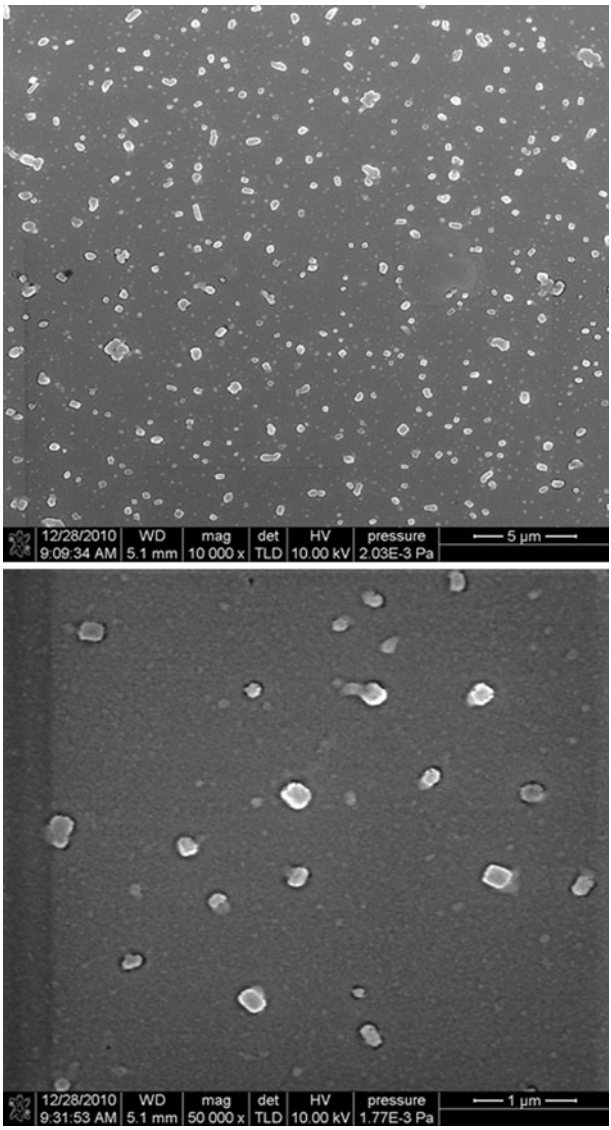

Fig. 3 SEM images of the MTX-loaded FA–CS nanoparticles (TPP/FA–CS mass ratio of 1:7)

nanoparticles. It indicates that MTX may exist as molecular dispersion in the polymeric nanoparticles.

Storage stability of the nanoparticles

Figure 6 shows the stability of the nanoparticles in 16 days monitored by relative light transmittance (T_i/T %; the transmittance of the FA–CS nanoparticles at each pH/transmittance at deionized water). All of the nanoparticles stored at different pH

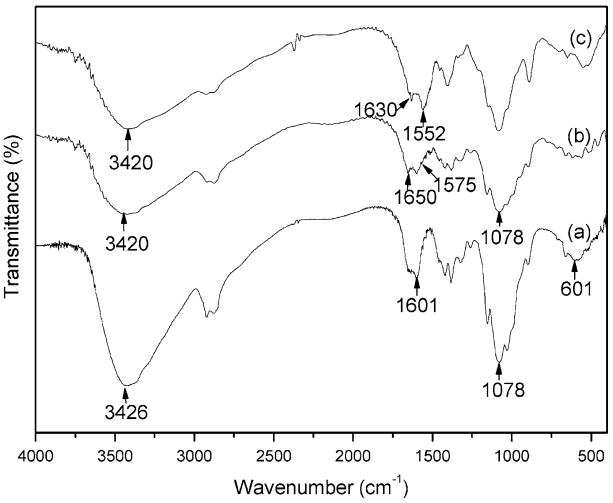

Fig. 4 FT-IR spectra of CS (*a*), FA–CS (*b*), and FA–CS nanoparticles (*c*)

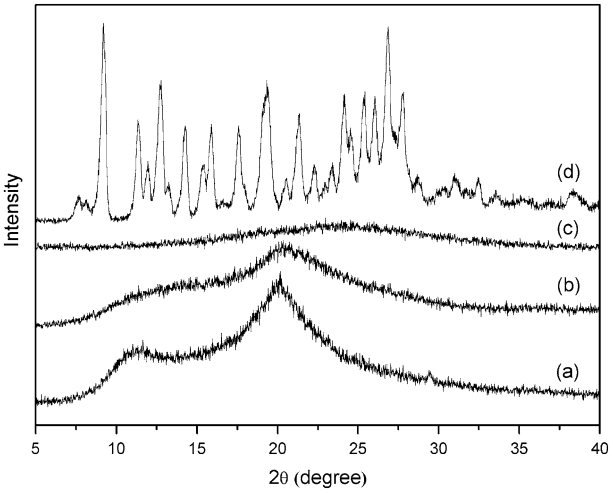

Fig. 5 XRD patterns of CS (*a*), FA–CS (*b*), MTX/FA–CS nanoparticles (*c*), and MTX (*d*)

showed no change in turbidity and preserved high stability in the entire pH range tested. But the T_i/T % of the FA–CS nanoparticles in different pH range slightly decreased compared to the nanoparticles stored in deionized water, which may be attributed to the change of the FA–CS surface charge in different pH conditions. As the increase of the solution pH, the protonation and surface charge of FA–CS decreased, which leads to the lower electrostatic repulsion among the FA–CS molecules. The nanoparticles had the tendency of slight particle aggregation, which decreased the transmittance of the suspension. But no obvious precipitation has been observed in the nanoparticle suspensions.

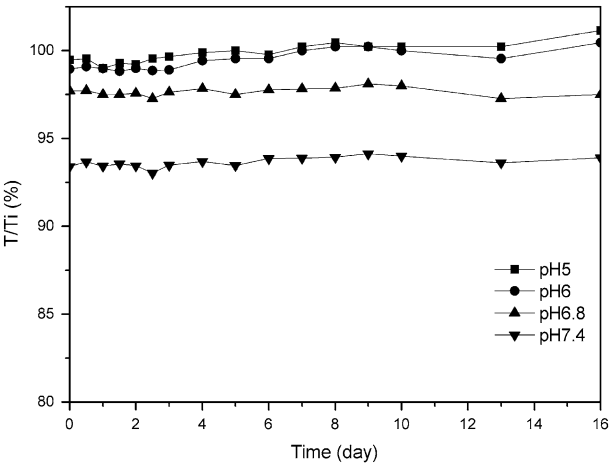

Fig. 6 Relative light transmittance (T_i/T %) of the FA–CS nanoparticles. T is the transmittance at 500 nm in deionized water and T_i is the transmittance at a given pH after nanoparticles have been stored for given days

In vitro release study

In vitro release studies of drug-loaded FA–CS nanoparticles and blank FA–CS nanoparticles without loading drug were carried out at pH 6.8 (Fig. 7). As the surrounding of tumor mass has a slightly acidic pH around 6.8, it is significative to study how the drug release profiles progress at this particular pH [29].

The in vitro cumulative release profiles of MTX from FA–CS nanoparticles with different drug-to-polymer ratios (from 1:20 to 4:20) are shown in Fig. 7. The release

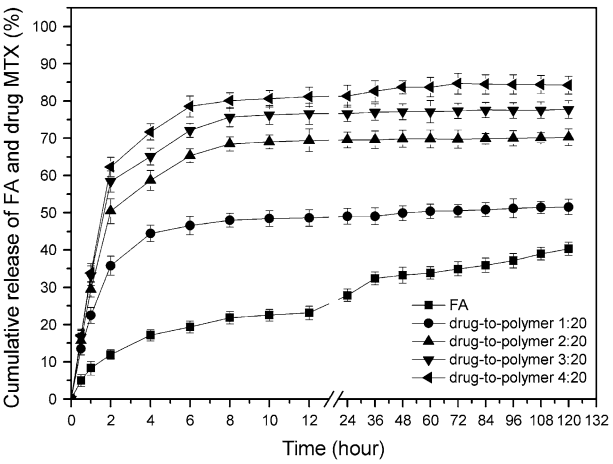

Fig. 7 Release curves of different feeding amount of MTX from the drug-loaded nanoparticles ($n = 3$) and the release of FA or low molecular weight FA conjugate fragments from the blank FA–CS nanoparticles

profiles depicts that the MTX release rate is highly influenced by the amount of MTX entrapped. As the drug-to-polymer ratio increased from 1:20 to 4:20, drug release rates also increased. The release behavior of the MTX-loaded nanoparticles exhibited three phases [30]. The first phase was a rapid release or burst release in the first 2 h. The rapid initial release involves the diffusion of the bound or adsorbed drug at the surface of nanoparticles. The second phase was a relatively slow release ranging from 2 to 8 h, which could be caused by a pore diffusion mechanism of the drug out of the nanoparticles. The third phase was a slower release which depended on the degradation of the polymer. The cumulative release of MTX-loaded nanoparticles with the drug-to-polymer ratio of 4:20 have shown 84% release whereas that of drug-to-polymer ratio of 1:20 nanoparticles have shown 51% at the end of the fifth day. It could be explained that drug in the nanoparticles might act as inert filler by occupying the available free volume of the swollen hydrogel and created a tortuous path for water molecules to permeate through [31]. Larger initial drug load of nanoparticles cause the faster movement of the water penetrating the surface of the drug-loaded nanoparticles and larger loading of the nanoparticles may also facilitate the relaxation of polymer chains.

In addition, published data supported the contention that neurotoxicity can be prevented by adequate FA or folinic acid rescue even after very high doses of MTX. In this nanoparticles system, FA not only acts as the targeting reagent in the drug delivery, but also could be used as a supplemental antidote in the treatment of MTX. The release curve of the blank FA–CS nanoparticles was also investigated (Fig. 7). The results of UV spectra show the appearance of the characteristic peaks of FA, indicating that FA or low molecular weight FA conjugate fragments could release from the nanoparticles with the degradation of copolymer. The released FA or low molecular weight FA conjugate fragments might have potential as supplemental antidote to prevent the neurotoxicity caused by MTX. Moreover, the previous studies [15] verified that the recovery effectiveness of FA in normal cells was more effective than in tumor cells because normal cells have lower polyglutamate synthetase activity. This release mechanism of FA or low molecular weight FA conjugate fragments might be utilized to reduce toxic effects of MTX to healthy tissues within the body.

Conclusions

To improve the tumor cell-selective targeting and prevent MTX-induced host toxicity, MTX encapsulated FA–CS nanoparticles were successfully prepared through a cross-linking approach with TPP. The nanoparticles were homogeneously dispersed with a narrow particle size distribution. Up to $11.54 \pm 0.31\%$ of MTX was encapsulated into the FA–CS nanoparticles. The in vitro release studies indicated that the amount of MTX entrapped highly influenced the release rate of MTX. FA or low molecular weight FA conjugate fragments could release from the blank nanoparticles which might be utilized as an antidote opportunely and greatly reduces toxic effects of MTX to healthy tissues within the body. These results

suggested that the FA–CS nanoparticles have highly promising potential as drug carrier system for the therapy of MTX in the cancer.

Acknowledgments This study was supported by the Fundamental Research Funds for the Central Universities of China (CDJXS10220008) and Key Scientific and Technological Projects of Chongqing Science and Technology Commission (CSTC2010AC5050).

References

1. Yang XD, Zhang QQ, Wang YS, Chen H, Zhang HZ, Gao FP, Liu LR (2008) Self-aggregated nanoparticles from methoxy poly(ethylene glycol)-modified chitosan: synthesis; characterization; aggregation and methotrexate release in vitro. Colloid Surf B 61:125–131
2. Seo DH, Jeong YIl, Kim DG, Jang MJ, Jang MK, Nah JW (2009) Methotrexate-incorporated polymeric nanoparticles of methoxy poly(ethyleneglycol)-grafted chitosan. Colloid Surf B 69: 157–163
3. Vauthier C, Dubernet C, Chauvierre C, Brigger I, Couvreur P (2003) Drug delivery to resistant tumors: the potential of poly(alkyl cyanoacrylate) nanoparticles. J Control Release 93:151–160
4. Gao XJ, Zhang XG, Zhang XJ, Cheng C, Wang Z, Li CX (2010) Encapsulation of BSA in polylactic acid-hyperbranched polyglycerol conjugate nanoparticles: preparation, characterization, and release kinetics. Polym Bull 65:787–805
5. Tang YF, Zhao YY, Li Y, Du YM (2010) A thermosensitive chitosan/poly(vinyl alcohol) hydrogel containing nanoparticles for drug delivery. Polym Bull 64:791–804
6. Torchilin VP (2006) Multifunctional nanocarriers. Adv Drug Deliv Rev 58:1532–1555
7. Jabr-Milane L, Vlerken LV, Devalapally H, Shenoy D, Komareddy S, Bhavsar M, Amiji M (2008) Multi-functional nanocarriers for targeted delivery of drugs and genes. J Control Release 130: 121–128
8. Chang YH, Xiao L, Du YM (2009) Preparation and properties of a novel thermosensitive *N*-trimethyl chitosan hydrogel. Polym Bull 63:531–545
9. Ji JG, Hao SL, Wu DJ, Huang R, Xu Y (2011) Preparation, characterization and in vitro release of chitosan nanoparticles loaded with gentamicin and salicylic acid. Carbohydr Polym 85:803–808
10. Popa MI, Lisa G, Aelenei N (2008) Thermogravimetric characterization of chitosan/alginate microparticles loaded with different drugs. Polym Bull 61:481–490
11. Agnihotri SA, Mallikarjuna NN, Aminabhavi TM (2004) Recent advances on chitosan-based micro- and nanoparticles in drug delivery. J Control Release 100:5–28
12. Kohler N, Sun C, Wang J, Zhang MQ (2005) Methotrexate-modified superparamagnetic nanoparticles and their intracellular uptake into human cancer cells. Langmuir 21:8858–8864
13. Theti DS, Jackman AL (2004) The role of α-folate receptor-mediated transport in the antitumor activity of antifolate drugs. Clin Cancer Res 10:1080–1089
14. Chan P, Kurisawa M, Chung JE, Yang YY (2007) Synthesis and characterization of chitosan-*g*-poly(ethylene glycol)-folate as a non-viral carrier for tumor-targeted gene delivery. Biomaterials 28:540–549
15. Cohen IJ (2004) Defining the appropriate dosage of folinic acid after high-dose methotrexate for childhood acute lymphatic leukemia that will prevent neurotoxicity without rescuing malignant cells in the central nervous system. J Pediatr Hematol Oncol 26:156–163
16. Cohen IJ (2007) Prevention of high-dose-methotrexate neurotoxicity by adequate folinic acid rescue is possible even after central nervous system irradiation. Med Hypotheses 68:1147–1153
17. Bayram M, Ozogul C, Ercan ZS, Dilekoz E, Soyer C, Bayram O (2006) Examination of the rescue effects of folic acid on derangement of the tubo-ovarian ultrastructural architecture caused by methotrexate. Adv Ther 23:772–777
18. Guo WJ, Hinkle GH, Lee RJ (1999) ^{99m}Tc-HyNIC-folate: a novel receptor-based targeted radiopharmaceutical for tumor imaging. J Nucl Med 40:1563–1569
19. Yang SJ, Lin FH, Tsai KC, Wei MF, Tsai HM, Wong JM, Shieh MJ (2010) Folic acid-conjugated chitosan nanoparticles enhanced protoporphyrin IX accumulation in colorectal cancer cells. Bioconjug Chem 21:679–689
20. Lee ES, Na K, Bae YH (2003) Polymeric micelle for tumor pH and folate-mediated targeting. J Control Release 91:103–113

21. Zhang ZP, Lee SH, Feng SS (2007) Folate-decorated poly(lactide-*co*-glycolide)-vitamin E TPGS nanoparticles for targeted drug delivery. Biomaterials 28:1889–1899
22. Wan AJ, Sun Y, Li HL (2008) Characterization of folate-graft-chitosan as a scaffold for nitric oxide release. Int J Biol Macromol 43:415–421
23. Lee DW, Lockey R, Mohapatra S (2006) Folate receptor-mediated cancer cell specific gene delivery using folic acid-conjugated oligochitosans. J Nanosci Nanotechnol 6:2860–2866
24. Duan JF, Du J, Zheng YB (2007) Preparation and drug-release behavior of 5-fluorouracil-loaded poly(lactic acid-4-hydroxyproline-polyethylene glycol) amphipathic copolymer nanoparticles. J Appl Polym Sci 103:2654–2659
25. Ji JG, Hao SL, Liu WQ, Wu DJ, Wang TF, Xu Y (2011) Preparation, characterization of hydrophilic and hydrophobic drug in combine loaded chitosan/cyclodextrin nanoparticles and in vitro release study. Colloid Surf B 83:103–107
26. de Moura MR, Aouada FA, Mattoso LHC (2008) Preparation of chitosan nanoparticles using methacrylic acid. J Colloid Interface Sci 321:477–483
27. Xu YM, Du YM (2003) Effect of molecular structure of chitosan on protein delivery properties of chitosan nanoparticles. Int J Pharm 250:215–226
28. Yoksan R, Jirawutthiwongchai J, Arpo K (2010) Encapsulation of ascorbyl palmitate in chitosan nanoparticles by oil-in-water emulsion and ionic gelation processes. Colloid Surf B 76:292–297
29. Dev A, Mohan JC, Sreeja V, Tamura H, Patzke GR, Hussain F, Weyeneth S, Nair SV, Jayakumar R (2010) Novel carboxymethyl chitin nanoparticles for cancer drug delivery applications. Carbohydr Polym 79:1073–1079
30. Agnihotri SA, Aminabhavi TM (2004) Controlled release of clozapine through chitosan microparticles prepared by a novel method. J Control Release 96:245–259
31. Rokhade AP, Shelke NB, Patil SA, Aminabhavi TM (2007) Novel interpenetrating polymer network microspheres of chitosan and methylcellulose for controlled release of theophylline. Carbohydr Polym 69:678–687